

1
2 **Separating annual, interannual and regional change in Sea Surface Temperature in**
3 **the Northeastern Atlantic and Nordic Seas**

Mischa J. M. Saes^{1†}, Caroline V. B. Gjelstrup¹, Andre W. Visser¹ and Colin A. Stedmon¹

5 ¹National Institute of Aquatic Resources, Technical University of Denmark, 2800 Lyngby,
6 Denmark

Corresponding author: first and last name (mischasaes@outlook.com)

† Current address: Danish Hydraulic Institute, Hørsholm, Denmark

9 **Key Points:**

- 10 • Seasonal fluctuations in Nordic Seas and Northeastern Atlantic sea surface temperatures
11 explains 90 % of the variability.
- 12 • Both summer maxima and winter minima are warming, with summer temperatures
13 warming twice as fast (0.4 and 0.2 °C per decade).
- 14 • Other sources of variability include sea-ice melt and switches in large-scale
15 oceanographic conditions in the Northeastern Atlantic.

This article has been accepted for publication and undergone full peer review but has not been through the copyediting, typesetting, pagination and proofreading process, which may lead to differences between this version and the [Version of Record](#). Please cite this article as doi: [10.1029/2022JC018630](https://doi.org/10.1029/2022JC018630).

This article is protected by copyright. All rights reserved.

16 **Abstract**

17 Sea surface temperature (SST) in the Northeastern North Atlantic and Nordic Seas exhibits
18 pronounced variability across seasonal to decadal time scales. These changes can be expected to
19 be driven by a combination of altered local conditions, shifts in seasonality and large scale
20 regional oceanographic change. Separating the contribution from each of these offers insight into
21 how the region is changing. Here, we present the result of an analysis of weekly satellite derived
22 SST data from 1979 to 2020. An empirical orthogonal function (EOF) analysis allows us to
23 separate observed changes in SST into independent underlying timeseries. Each timeseries
24 explains part of the variability in SST. EOF1 can be allocated with changes in seasonality and a
25 long-term warming trend, with summer maxima warming with twice the rate ($0.043\text{ }^{\circ}\text{C yr}^{-1}$)
26 compared to winter minima ($0.023\text{ }^{\circ}\text{C yr}^{-1}$). EOF2 is associated with the North Atlantic subpolar
27 gyre and the North Atlantic Oscillation, affecting the Atlantic Water flow across the Greenland-
28 Scotland Ridge, imposing a di-pole cooling/warming pattern. Local sea-ice melt along the
29 southeast Greenland shelf is represented by EOF3, and finally the influx of warmer water with
30 the North Icelandic Irminger Current is captured by EOF4. Each of these disaggregated signals
31 differ considerably in their contribution to driving temporal and spatial trends in SST. The
32 isolated signals offer a high-resolution long time series of valuable indicators of oceanographic
33 change which will likely be reflected in biogeochemistry, plankton, fish, mammals, and seabirds
34 in the region.

35

36 **Plain Language Summary**

37 Sea surface temperature (SST) can be measured by sensors mounted on satellites and this
38 provides a dataset with exceptional regional and temporal coverage from 1979 to present. Here
39 our focus is on examining oceanographic change in the Northeastern Atlantic and Nordic Seas,
40 bordering Greenland, Iceland and Norway. We apply a data analysis technique that allows us to
41 separate the variability in SST in the region into a series of underlying factors. With this we can
42 resolve: how the seasonal winter minimum temperatures and summer maximum temperatures
43 have been increasing; how conditions in the North Atlantic are driving changes in the region;
44 how increased sea-ice melt is influencing SST; and finally trace the occurrence and impact of an
45 abrupt inflow of warmer water northwards along the west coast of Iceland. Combined these

46 disaggregated factors may help explain changes in the distribution and structure of the marine
47 ecosystem in the region.

48 **1 Introduction**

49 Sea surface temperature (SST) measured by satellites provides a unique time series with high
50 temporal and geographical resolution unparalleled to many other essential ocean variables.

51 Despite its limited penetration depth it can be used as a proxy for the ocean heat content of the
52 mixed layer (Chen & Tung, 2018). As a result, variations in SST can be linked to changing
53 positions of oceanographic fronts (Sutherland & Pickart, 2008; Raj et al., 2019), variability in
54 upwelling (Lentz & Largier, 2006) or deep convection (de Jong & de Steur, 2016) and warming
55 of surface waters as a result of climate change (Masson-Delmotte et al., 2019). Variations in SST
56 can also indicate initiation of larger changes in regional marine ecosystems as oceanographic
57 change can have a cascading impact on all trophic levels in ecosystems (Hátún et al., 2009).

58 The Northeastern Atlantic and Nordic Seas are characterized by distinctive domains in
59 the average SST and its variability (Fig. 1 and 2). The shelf waters in the west are influenced by
60 Polar Waters brought south from the Arctic Ocean with the East Greenland Current (EGC). SST
61 is cold either due to its Arctic origin, or contribution from seasonal ice melt from both sea-ice
62 and the Greenland ice sheet. Part of the southward flowing surface EGC deviates eastward,
63 where it affects the surface waters in the Nordic Seas (Jeansson et al., 2017). Once past the
64 Denmark Strait, the EGC is confined to the shallow, narrow region along the southeast
65 Greenland coast. Further inshore, a low salinity southward flowing surface jet known as the East
66 Greenland Coastal Current (EGCC) resides (Sutherland & Pickart, 2008; Bacon et al., 2014).

67 In the eastern part of the region surface waters are dominated by the comparatively warm
68 and saline Atlantic Water (AW) flowing poleward with the North Atlantic Current (NAC). Part
69 of this current continues northwards into the Norwegian Sea as the Norwegian Atlantic Current
70 (NwAC) inducing a strong SST gradient across the Nordic Seas (Fig. 1) (Orvik and Niiler 2002).
71 Some of the NwAC diverges into the Barents Sea, while the remainder continues north entering
72 the Arctic Ocean via the West Spitsbergen Current (WSC) in the Fram Strait (Orvik and Niiler
73 2002). Here, about half of the flow recirculates turning west and merging with the EGC to

74 continue southwards as Return Atlantic Water (Bourke et al., 1988; Hatterman et al., 2016;
75 Jeansson et al., 2017; Raj et al., 2019).

76 The region south of the Greenland-Scotland Ridge (GSR) is dominated by the cyclonic
77 Subpolar Gyre (SPG). The NAC comprises the southern and eastern boundary currents of the
78 gyre. As the NAC enters the Subpolar North Atlantic (SPNA) it separates into branches; one
79 flows over the Rockall Plateau and the Rockall Trough between Iceland and Ireland, one enters
80 the Iceland Basin and one recirculates southward to eventually re-join the subtropical gyre (STG)
81 (Daniault et al., 2016). The Irminger Current (IC) separates from the northward flow in the
82 Iceland Basin and turns westward towards east Greenland. South of the Denmark Strait, the IC
83 bifurcates with a smaller portion flowing northwards through Denmark Strait and along the
84 western and northern coast of Iceland as the North Icelandic Irminger Current (NIIC). The larger
85 part turns south and flows along the east Greenland shelf break parallel to the EGC. Sharp
86 oceanic fronts develop between the IC, EGC and EGCC (Hátún et al., 2005). A portion of this
87 flow will remain in the Irminger Sea, as it recirculates near Cape Farewell, whilst another portion
88 will round Cape Farewell to continue north along western Greenland.

89 In addition to advection of ocean currents, SST in the Northeastern Atlantic and Nordic
90 Seas is strongly influenced by heat exchange with the atmosphere, sea-ice and associated melt
91 water, and upward heat fluxes from deeper warm waters (Fuervik, 2000; Carvalho & Wang,
92 2020). Based on the HadISST dataset, Meredith et al., (2019) show a warming trend in the
93 Northeastern Atlantic and Nordic Seas over the 1982-2017 period. Barton et al., 2018 and
94 Asbjørnsen et al., (2020) also show recent SST increase in the northern Nordic Seas and Barents
95 Sea. In contrast, the Irminger Sea experienced a decline in SST between 2007 and 2016 (Broome
96 et al., 2020; Fig. 2), indicating a disconnect between the Northeastern Atlantic and Nordic Seas
97 over this period. A linear regression analysis of SST over the 2007-2020 period clearly reflects
98 these patterns in the region (Fig. 2). In the Greenland Sea, the warming trend can be up to 0.15
99 °C per year and appears to be persistent across the year. South of Iceland, significant cooling
100 over the SPG is apparent. The observed cooling is largest in summer, with rates towards -0.15 °C
101 per year (Fig. 2). Regions where no significant linear relationship is found (yellow patterns in
102 Fig. 2) clearly reveal the frontal zones between water masses (Orvik and Niiler 2002), in
103 particular boundaries of the EGC and EGCC towards the west and the propagation northwards

104 and subsequent dissipation of a front in the southeast of the region during the transition from
105 winter to summer (Fig. 2).

106 Several mechanisms have been invoked to explain the observed trends in regional water
107 temperatures. These include large scale atmospheric forcing such as the North Atlantic
108 Oscillation (NAO), fluctuations in the SPG circulation, changing wind speeds, and variable sea-
109 ice concentration (Furevik, 2000; Broome et al., 2020; Carvalho & Wang, 2020). The aim of
110 this study is to carry out a holistic analysis of SST of the region by applying an Empirical
111 Orthogonal Function (EOF) analysis also known as a Principle Component Analysis. SST is
112 hypothesized to be responding to a combination of altered local conditions, potential shifts in
113 seasonality and large scale regional oceanographic change, which will materialize as a linear
114 combination of factors influencing surface water heat content. The analysis allows us to isolate
115 the contribution of underlying independent (orthogonal) factors to the observed SST changes
116 with no assumption on temporal or regional trends. Separating the contribution from each of
117 these offers insight into how the region is changing and also offers factors which we propose can
118 be linked to additional shifts in distribution and diversity of marine organisms, from
119 phytoplankton up to marine mammals.

120 **2 Materials and Methods**

121 The region of interest expands between 48 °W and 9 °E, and 58 °N to 82 °N. Two Copernicus
122 SST datasets with coverage of the region were used in the analysis (Table 1). The first was a
123 near-real time data product derived across different satellite platforms called “Operational Sea
124 Surface Temperature and Sea Ice Analysis (OSTIA)”, developed by the Met Office. The product
125 is identified as “SST_GLO_SST_L4_NRT_OBSERVATIONS_010_001” (Donlon et al., 2012;
126 Good et al., 2020; Stark et al., 2007). It uses satellite data provided by the GHRSSST framework
127 (Group for High Resolution SST) and has global coverage on a 0.05° (approximately 6 km along
128 the north-south axis in region of interest, and between 800 m and 3 km in the east-west direction)
129 resolution grid and includes daily sea surface foundation temperature data (temperature of upper
130 10 m of the ocean, free of diurnal temperature variations), sea-ice cover and analysis error for the
131 2007-2020 period. In order to remove bias errors, the satellite observed SST has been compared
132 with in-situ SST measurements (drifting buoys) and ENVISAT Advanced Along Track Scanning

133 Radiometer (AATSR) SST observations (Donlon et al., 2012). As a result, an uncertainty value
134 (in Kelvin), is provided for each location at every time step. The high spatial resolution allows
135 one to identify fine structures in the position of fronts (Fig. 2).

136 To extend the temporal coverage to 1979, the ERA5 reanalysis dataset provided by the
137 European Centre for Medium-Range Weather Forecasts (ECMWF) and available via Copernicus
138 Climate Change Service data portal was used (Hersbach et al., 2018). This dataset is derived
139 from a combination of observational and model data to form a complete spatial and temporal
140 series provided at 0.25° (approximately 27 km in the region of interest along the north-south
141 axis, and between 4 km and 15 km) horizontal and hourly temporal resolution (Dee et al., 2014).

142 2.1 Data pre-processing and EOF analysis

143 In contrast to the linear regression analysis (Fig. 2), EOF analyses cannot be applied to data sets
144 with missing data points. While interpolation with bordering (temporal and spatial)
145 measurements can produce visually acceptable results, they do not actually aid the EOF analysis
146 by providing additional information. In fact, this can potentially impair the separation of
147 underlying features as signal noise and variability is averaged and combined. Missing data in the
148 near real time (NT) dataset stems for the most part from the presence of sea-ice. Before EOF
149 analysis, all data points with a sea-ice fraction greater than 25 % were discarded. These
150 corresponded to data points already flagged with a high measurement error. An ice mask was
151 then generated which excluded data from areas where there has been ice coverage. Due to the
152 inclusion of models, the ERA5 dataset extrapolates below the sea-ice, offering the potential to
153 include ice covered waters, thereby introducing a discrepancy in EOF results from the two
154 datasets. The application of an identical ice mask to both datasets resulted in comparable EOFs
155 (Fig. S1 to S4). As the ERA5 dataset has superior temporal coverage the EOF analysis presented
156 from here onwards is based on the ERA5 reanalysis. The data was down-sampled to weekly
157 averages and organized into a matrix with geographical location as columns and temporal series
158 as rows. Before performing the EOF analysis the data was centered (mean subtraction) and

159 scaled (normalized to standard deviation) by location to ensure equal weighting of data from
160 different regions.

161 With the EOF analysis, we separate SST variability in space and time into a number of
162 orthogonal components each having a geographical loading and a temporal score. The product of
163 the loadings map, score time series for a given component and the standard deviation map of the
164 original data allows us to back-calculate the temperature variation represented by the component
165 (i.e. the given components contribution to temperature anomaly).

166 2.2 Climate variables

167 To assess the potential driving forces of the temporal development in the EOFs, several climate
168 indices were gathered. A SPG index based on multiple linear regression of the first and second
169 modes of North Atlantic sea surface height variability was used as an indicator of the strength
170 and shape of the subpolar gyre. The index was derived by Chafik in (2019) and gathered from
171 the Bolin Center for Climate research: <https://bolin.su.se/data/chafik-2019-3>. The North Atlantic
172 Oscillation (NAO) index is based on the atmospheric pressure difference between Iceland and
173 the Azores and conditions in the study region can potentially be correlated to this as it influences
174 North Atlantic temperature and precipitation patterns (Barnston & Livezey, 1987; Hurrell, 1995;
175 van den Dool et al., 2000; W. Y. Chen & van den Dool, 2003). A monthly time series of the
176 NAO index was obtained from NOAA.

177 3 Results

178 Almost 95 % of the observed variation in SST is explained by the first four components
179 from the EOF analysis (Fig. 3). Systematic patterns in their geographic distribution and temporal
180 signal indicate that they are linked to specific phenomena and offer confidence in the robustness
181 of the result. The robustness of the derived EOF components was further confirmed by re-
182 running the EOF decomposition on de-seasoned SST, which resulted in comparable components
183 (Fig. S5). The largest portion (90 %) of the variability in the region can be attributed to seasonal
184 warming and cooling. The EOF1 loading map is largely featureless (Fig. 3a) indicating that this
185 component is of equal importance for the entire study area and likely driven by atmospheric
186 forcing. The one exception is a narrow band along the edge of the sea-ice mask, where the

187 loading is slightly lower. A reconstruction of SST anomalies imposed by this component (Fig.
188 3b) shows a strong imprint of seasonality with variability around the mean of more than 6 °C. In
189 order to assess if there has been a change in the timing and intensity of seasonal maxima and
190 minima, the temperature anomaly for EOF1 was plotted by year and week (Fig. 4a). A regression
191 analysis indicates that there has been no significant change in timing across the years (p-value
192 >0.05), as would be expected. Also apparent is a positive linear trend in both the summer
193 maximum (0.043 °C yr⁻¹) and winter minimum (0.024 °C yr⁻¹) SST (Fig. 4b). Note, that the rates
194 provided on Fig. 4 were calculated specifically for the Irminger Sea location, but are very similar
195 across the entire region as the EOF1 loadings are evenly distributed (Fig. 3a). These results show
196 that SST increased with twice the rate in summers compared to winters over the course of 41
197 years.

198 The time series associated with EOF1 is also characterized by a shift towards higher
199 temperatures in 2000 that persists through to the end of the time series (Fig. 4c). A Chow test
200 was done to gauge whether the EOF1 time series is best described with a single linear regression
201 model through the entire time series (Fig. 4b), or if the description of the time series significantly
202 improves when using two regression models, one on either side of the identified shift. The Chow
203 test concludes that the time series representation is significantly better when sectioned into two
204 around August 2000 (Fig. 4c) (p-value < 0.01), thus confirming the existence and timing of the
205 identified shift.

206 The second EOF explains approximately 2.6 % of the observed variation in SST and is
207 opposite in sign pivoting north-south approximately at the latitude of Iceland. This spatial pattern
208 has a high degree of similarity to the linear trends presented in Fig. 2. This gives confidence that
209 the dipole nature of EOF2 is a real feature of SST variability in the Northeast Atlantic rather than
210 an artefact introduced by the constraints of the EOF approach itself. The reconstructed SST
211 anomalies from EOF2 show a contribution to SST variability of more than 2°C. The time series
212 is characterized by three periods: i) a period from 1979 to 1995 where there are variable
213 anomalies; ii) a period from 1995 to 2014 where temperature anomalies in the north are and
214 remain persistently colder, and conversely persistently warmer in the south; and iii) a period
215 from 2014 to 2020 where anomalies changed to be persistently warmer and cooler in the north
216 and south respectively. These fluctuations hint at a possible linkage to regional climate indices

217 such as the SPG and NAO indices. A correlation analysis found relations between EOF2 scores
218 and both the NAO (-0.41, p-value < 0.01) and the SPG (-0.67, p-value < 0.01) indices at five and
219 four weeks lag respectively (Fig. 5). Lag times with the highest correlation were determined
220 from cross-correlation analysis. It is clear that the segregations of the time series of EOF2 into
221 three periods agrees with trends in the two indices (Fig. 5). In particular the middle period
222 spanning from 1995 to 2014 where the NAO and SPG indices are persistently negative, and the
223 final period where there is a systematic change to positive values (note both indices are plotted
224 with inverted axes in Figure 5b and d).

225 Variability in SST within a narrow band spanning the length of the southeast Greenland
226 shelf was captured by EOF3, which contributes 1.2 % of the total variation in SST (Fig. 3e). This
227 band broadly corresponds to the area with low seasonality (EOF1, Fig. 3a), indicating that it has
228 a more unique variability not directly related to the large-scale seasonal warming and cooling
229 explained by EOF1. Fig. 3f indicates that these waters have experienced a systematic long-term
230 warming across much of the time series, in particular from the late 1980s (approximately 1 °C
231 increase over a 40 year period). Furthermore, reconstructed SST also indicates high frequency
232 variability linked to seasonal trends (Fig. 6). The SST anomaly explained by EOF3 is lowest in
233 summer months within the band of high loadings along the edge of the sea-ice mask (Fig. 6). An
234 analysis of the timing of the summer minimum (similar to that done for EOF1) indicated that
235 there has been no significant systematic shift over the time period. As can be seen in Fig. 6 the
236 timing of the minimum is variable and ranges between late May and late June. Both the seasonal
237 maxima and minima experience a comparable SST increase (e.g. 0.025 and 0.022 °C yr⁻¹
238 respectively at 65 °N 30 °W) through the entire 41 year study period, indicating that the long-
239 term trend is the same for both summer and winter. The intensity of this long-term trend,
240 however, varies spatially as reflected in the EOF3 loading (Fig. 3f).

241 The fourth EOF is largely confined to the region along the Greenland-Faroe Islands ridge
242 with greatest values northwest and southeast of Iceland (Fig. 3g). Fig. 3h shows the time series
243 of the SST anomaly explained by EOF4 for two selected points, one near Denmark Strait and
244 another in the Greenland Sea. From this, it is clear that EOF4 is focused on the changes
245 occurring in Icelandic waters (red line in Fig. 3h). The time series is characterized by two
246 frequencies: a high frequency variability which was found not to be linked to seasonality; and a

247 lower frequency change. The latter appeared to represent somewhat stable conditions before
248 2003, a positive excursion in SST up to 2 °C between 2003 and 2005 followed by a brief return,
249 then a persistently positive SST anomaly from 2007 onwards (Fig. 3h). The 2007 shift is
250 confirmed by a change point detection procedure similar to that done for EOF1. Comparison of
251 this time series with measurements from the Icelandic monitoring program indicates that the
252 warm SST anomaly in 2003 and 2004 captured in EOF4 corresponds well with observations as
253 supported by a relatively high correlation coefficient ($R^2 = 0.47$, p-value = 0.02; Fig. 7).

254 **4 Discussion**

255 The decomposition of SST into its linear components has partitioned SST changes into that due
256 to altered seasonality captured in EOF1 and EOF3 and that linked to variable oceanic advection
257 captured in EOF2 and EOF4.

258 **4.1 Seasonal control of SST**

259 The seasonal warming and cooling of the ocean surface is the major determinant of SST
260 variability in the SPNA and Nordic Seas. Although the timing of the seasonal maximum and
261 minimum has not changed over the forty-year period considered here, the intensity of seasonal
262 warming and cooling has (Fig. 3). Annually the region is a net source of heat to the atmosphere
263 (Serreze et al., 2007). Cooling of surface waters from September to March exceeds the warming
264 that occurs from April to August (Serreze et al., 2007). EOF1 indicates that winter SST has been
265 rising at a rate of 0.024 °C per year and summer SST at a rate approximately twice that
266 throughout the region. These warming rates are in good agreement with those reported for March
267 (0.2°C per decade) and September (0.4 °C per decade) over the period 1982-2017 in Meredith et
268 al. (2019). The findings reveal two changes that are occurring in the seasonal component of SST
269 in the region. The fact that summer and winter temperatures are increasing suggests that there is
270 a general increase in heat transport into the region. However, this does not explain why summer
271 maxima are warming faster than winter minima. This could in turn be reflecting a decrease in the
272 summer mixed layer depth. As SST increases the mixed layer depth can be expected to shoal,

273 assuming that the warming of surface water dominates the density change, rather than change at
274 depth (Somavilla et al., 2017).

275 Strong seasonal variability is also evident in the annual build-up and melt of sea-ice.
276 Summertime sea-ice melt along the east Greenland shelf absorbs considerable amounts of latent
277 heat, and releases cold, fresh waters initially lowering summer SST in the western part of the
278 Nordic Seas (Smedsrud et al, 2022). This is reflected in the high frequency signal captured in
279 EOF3 (Fig. 6). This component thereby serves as a local, geographical correction to the seasonal
280 pattern identified by EOF1. Since EOF3 mainly serves as a summertime correction, it should not
281 be seen as an absolute summer cooling. It merely modifies the seasonal trend in EOF1 to
282 represent a local delay/reduction of the summer heating along the ice front, possibly due to sea-
283 ice meltwater or polar waters transported in the EGC. The general increase in SST along east
284 Greenland observed in EOF3 (apparent as a baseline shift in Fig. 6) is comparable to that seen
285 for winter SST in EOF1. The similarity of the interannual trends embedded in EOF1 and EOF3
286 suggests that these components have a common driver.

287 4.2 Regional connectivity

288 Although seasonal heating and cooling of the surface drives the majority of SST variability,
289 advection of warm, saline AW into the Nordic Seas is responsible for imposing important
290 regional differences. Since EOF1 represents seasonal variability, it is reasonable to assume EOFs
291 2 and 4 to be related to oceanic advection and interannual variability, which will be considered in
292 the following. AW exchange between the SPNA and Nordic Seas is facilitated via three main
293 inflow pathways: i) flow through the Faroe-Shetland Channel, ii) flow between Iceland and the
294 Faroe Islands and iii) inflow with NIIC through Denmark Strait (Hansen and Østerhus, 2000;
295 Østerhus et al., 2019). All three inflow pathways contribute to the substantial increase (21 TW)
296 in ocean heat transport in 1998-2002 identified in Tsubouchi et al., (2021). The authors
297 furthermore characterize this abrupt increase as a change-point similar to that reported for EOF1
298 in the current study (Fig. 4c & Fig. S2) suggesting that the identified 2000 shift in EOF1
299 represents increased oceanic heat transport across the GSR. As part of the variability in the
300 inflow of warm waters is set upstream in the NAC, one can expect variability in the three inflows
301 to be correlated and resolved as a single EOF. This is for the most part true, as seen for EOF2,

302 however the isolation of an additional contribution, more specific to the NIIC (EOF4), reveals a
303 local component which is not directly correlated.

304 Although AW transport with the NIIC is the smallest of the three through-flows, it is the
305 primary source of heat and nutrients to the north Iceland shelf (Fig. 1; Hansen and Østerhus,
306 2000). High variability due to translation of fronts is inherent to this area (Fig. 2e-h), and
307 fluctuations in the temperature and volume of the AW inflow with the NIIC have been used to
308 explain variable temperature and heat transport to the shelf (Jónsson and Valdimarsson, 2012;
309 Zhao et al., 2018; Casanova-Masjoan et al., 2020). Based on mooring observations Jónsson and
310 Valdimarsson (2012) captured an anomalously strong NIIC inflow event between 2003 and
311 2004, which concurs with the temperature excursion in the fourth component derived here (Fig.
312 7). Previous studies concerning the NIIC furthermore document a shift to persistently elevated
313 temperatures after 2007 compared to conditions before the 2003 warm event (Zhao et al., 2018;
314 Casanova-Masjoan et al., 2020). A similar shift was noted in EOF4 (Fig. 7), which supports our
315 interpretation of EOF4 as representative of AW inflow with the NIIC.

316 East of Iceland, the NwAC carries heat and salt across the Iceland-Scotland ridge and
317 into the Norwegian Sea. Consistent with numerous previous studies relating interannual
318 variability in inflow properties and volume to large-scale wind forcing patterns (e.g. Sandø et al.,
319 2012; Bringedal et al., 2018), we found a significant correlation (-0.41 , p -value < 0.01) between
320 NAO and EOF2 (Fig. 5d). Strengthened westerlies under positive NAO cause elevated heat loss
321 and negative SST anomalies over the SPNA (Visbeck et al., 2003; Sarafanov 2009).
322 Simultaneously, the intensified atmospheric circulation transports more warm, moist air
323 northwards and increases AW inflow with the NwAC, invoking positive SST anomalies in the
324 eastern Nordic Seas (Furevik, 2000; Dickson et al., 2000; Mikailova et al., 2021). As
325 demonstrated by Deser et al., (2010), a dipole SST pattern between the SPNA and Nordic Seas
326 consequently develops under positive NAO forcing. Whilst the correlation between NAO and
327 EOF2 is significant, the robustness of this relationship is questionable as the strength of
328 correlation is highly sensitive to the length of the smoothing window.

329 Other studies have attributed variable inflow properties to changes in the strength and
330 shape of the SPG (e.g. Hátún et al., 2005; Lozier & Stewart, 2008; Kenigson & Timmermans,

331 2021). A strong correlation (-0.67 , p -value < 0.01) with the SPG index suggests that SPG
332 dynamics are indeed manifested in the development of regional SST patterns (Fig. 5). Shifts in
333 the position of the subarctic front, commonly referred to as expansion/contraction of the SPG
334 have been invoked to explain decadal temperature trends in the SPNA and variable composition
335 of inflow across the GSR (Hátún et al., 2005; Desbruyères et al., 2021; Kenigson &
336 Timmermans, 2021). Weak SPG circulation is associated with contraction of the SPG and
337 expansion of the STG, effectively displacing the subarctic front northwestwards, and allowing
338 for a wider passage for warm, saline subtropical waters to penetrate the eastern SPNA and flow
339 into the Nordic Seas (Häkkinen et al., 2011). Conversely, during strong SPG circulation,
340 subtropical waters are blocked by the now expanded SPG, rerouting the subtropical waters
341 southwards (Häkkinen & Rhines, 2004). The Atlantic inflow to the Nordic Seas is in this case
342 comprised of an increased ratio of cold, fresh SPNA source waters compared to STG waters.
343 Accordingly, the SPG index and SST anomalies in the SPNA are inversely correlated in
344 agreement with Hátún et al., (2005).

345 However, whilst the SPNA has been cooling since the mid 2000's in accordance with the
346 expanded state of the SPG, the Nordic Seas have not (Fig. 2 and Fig. 5). A possible explanation
347 for this apparent disconnect is that the SPNA cooling had simply not reached the Nordic Seas by
348 2014. According to Holliday et al., (2008) NAC anomalies are detectable in the southern
349 Norwegian Sea approximately one year after crossing the Faroe-Shetland Channel, and appear
350 south of Svalbard three years later. In another study, Kenigson and Timmermans (2021) suggest
351 a lag of five years between the development of freshwater content anomalies in the SPNA and a
352 measurable change in the Nordic Seas. It is therefore possible that the dipole fingerprint
353 associated with EOF2 is the consequence of slow propagation and mixing time scales of
354 temperature anomalies generated by changing states of the SPG. Broomé et al., (2020) offer an
355 alternative explanation for the SPNA-Nordic Seas disconnect. The authors suggest that the
356 connection between the SPNA and Nordic Seas is time varying as they show that correlation
357 between temperature in the eastern Nordic Seas and SPNA is only significant along the
358 subtropical AW pathway. Thus, the SPNA-Nordic Seas connection is strong under contracted

359 gyre conditions but not when the SPG is expanded. This notion highlights that SPNA and Nordic
360 Seas exchanges across the GSR are not yet fully understood (Bringedal et al., 2018).

361 In contrast to the derived EOFs, the physical processes driving observed changes are not
362 necessarily independent (orthogonal) of each other. Therefore, it is possible that both NAO and
363 SPG associated changes are manifested in EOF2. Whilst we have only speculated the mechanism
364 causing the dipole spatial pattern associated with EOF2, it is clear that AW inflow patterns are
365 important drivers of SST variability in the SPNA and Nordic Seas.

366 The increased ocean heat transport as represented by the shift in EOF1 in 2000 and the
367 de-seasoned EOF model (Fig. S2), the “switching” role of the SPG and increased AW inflow
368 with the NIIC, collectively suggest an increase in the oceanic heat transport to the Nordic Seas
369 over the 1979-2020 period. These findings are aligned with a suite of recent studies on the heat
370 budget of the Nordic Seas recently reviewed by Smedsrud et al., (2022) and provide a separation
371 of the response in SST into independent underlying factors. Increases in AW inflow in part
372 contradict evidence for decreases in Atlantic meridional overturning circulation (AMOC) (e.g.
373 Smeed et al., (2018)), which are based on deepwater moorings further south. This apparent
374 disconnect between observations from the subtropics and Nordic Seas is also noted in Tsubouchi
375 et al., (2021) and highlights the fact that linkages between the subtropics and higher latitudes are
376 yet to be resolved.

377 **5 Conclusions**

378 Sea surface conditions are the result of the complex interplay between atmosphere and ocean.
379 SST's are subjected to large scale atmospheric patterns (e.g. NAO), short term cycles (e.g.
380 day/night cycles), intermediate term cycles (e.g. seasonal) cycles and long term cycles (e.g.
381 strengthening and weakening of the AMOC). Our results show that EOF analysis is a robust
382 method for disentangling both spatial and temporal patterns in SST, enabling us to attribute
383 change to specific processes acting on various timescales and differing in geographic extents.
384 This has implications for the predictability of SST conditions and their impacts in the
385 Northeastern Atlantic and Nordic Seas. From the EOF analysis, we isolate a dominant seasonal
386 signal revealing that summer maximum SST is increasing at about twice the rate of winter
387 minima warming (EOF1), potentially reflecting a shallowing of the summer mixed layer depth.

388 Furthermore, the impact of NAO and the SPG on regional SST is isolated (EOF2). This is of
389 major importance as it impacts the intrusion of warm AW into the Nordic Seas with consequence
390 for climate and ecosystems in the region. More local effects on SST, such as the impact of sea-
391 ice melt along the ice edge were also captured in the analysis (EOF3). Finally, EOF4 relates to
392 variable AW heat transport onto the north Iceland shelf with the NIIC.

393 The influence of each of these independent SST components on regional SST trends
394 varies considerably throughout the region and across the time period considered. Individually,
395 the EOF components pose as high-resolution time series of oceanographic change that is likely
396 also reflected in biogeochemistry, plankton, fish, mammals and seabirds in the region. We
397 therefore suggest that some of EOF components presented here may provide useful proxies:
398 EOF3 may be regarded as an indirect indicator of the impact of sea-ice melt, whereas EOF4
399 represents a proxy for influx of warm nutrient-rich AW to the north Iceland shelf.

400 **Acknowledgments**

401 C. A. S. acknowledges received funding from the Independent Research Fund Denmark Grant
402 No. 9040-00266B and the Nordic Council of Ministers AG-Fisk Grant number (209)-2020-
403 LEGCO. A.W.V acknowledges funding from Horizon2020 Project ECOTIP (Grant agreement
404 #869383).

405

406 **Open Research**

407 The OSTIA and ERA5 datasets used in this paper are available from at:

408 <https://doi.org/10.48670/moi-00165> and <https://doi.org/10.24381/cds.adbb2d47>, respectively.

409 CTD data from the Siglunes section and the first four EOF components derived are freely
410 available at data.dtu.dk via DOI 10.11583/DTU.19316264.

411

412 **References**

413 Asbjørnsen, H., Årthun, M., Skagseth, Ø., & Eldevik, T. (2020). Mechanisms Underlying Recent
414 Arctic Atlantification. *Geophysical Research Letters*, 47(15).
415 <https://doi.org/10.1029/2020GL088036>

416

417

418

419 Bacon, S., Marshall, A., Holliday, N. P., Aksenov, Y., & Dye, S. R. (2014). Seasonal variability
420 of the East Greenland Coastal Current. *Journal of Geophysical Research: Oceans*, 119(6), 3967–
421 3987. <https://doi.org/10.1002/2013JC009279>

422

423 Barnston, A. G., & Livezey, R. E. (1987). Classification, seasonality and persistence of low-
424 frequency atmospheric circulation patterns. *Monthly Weather Review*, 115(6), 1083–1126.
425 [https://doi.org/10.1175/1520-0493\(1987\)115<1083:CSAPOL>2.0.CO;2](https://doi.org/10.1175/1520-0493(1987)115<1083:CSAPOL>2.0.CO;2)

426

427 Bringedal, C., Eldevik, T., Skagseth, Ø., Spall, M. A. & Østerhus, S. (2018). Structure and
428 Forcing of Observed Exchanges across the Greenland-Scotland Ridge. *Journal of Climate*,
429 31(24), 9881-9901. <https://www.jstor.org/stable/26661469>

430

431 Broomé, S., Chafik, L., & Nilsson, J. (2020). Mechanisms of decadal changes in sea surface
432 height and heat content in the eastern Nordic Seas. *Ocean Science*, 16(3), 715-728.

433 <https://doi.org/10.5194/os-16-715-2020>

434

435 Bourke, R. H., Weigel, A. M., & Paquette, R. G. (1988). The Westward Turning Branch of the
436 West Spitsbergen Current. In *Journal of Geophysical Research*, 93.

437 <https://doi.org/10.1029/JC093iC11p14065>

438 Barton, B. I., Lenn, Y. D., & Lique, C. (2018). Observed Atlantification of the Barents Sea
439 Causes the Polar Front to Limit the Expansion of Winter Sea Ice. *Journal of Physical*
440 *Oceanography*, 48(8), 1849–1866. <https://doi.org/10.1175/JPO-D-18-0003.1>

441

442

443

444 Carvalho, K. S., & Wang, S. (2020). Sea surface temperature variability in the Arctic Ocean and
445 its marginal seas in a changing climate: Patterns and mechanisms. *Global and Planetary Change*,
446 193, 103265. <https://doi.org/10.1016/J.GLOPLACHA.2020.103265>

447

- 448 Casanova-Masjoan, M., Pérez-Hernández, M. D., Pickart, R. S., Valdimarsson, H., Ólafsdóttir,
449 R. S., Macrander, A., Grisolia-Santos, D., Torres, D. J., Jónsson, S., Våge, K., Lin, P. &
450 Hernández-Guerra, A. (2020). Along-stream, Seasonal, and Interannual Variability of the North
451 Iceland Irminger Current and East Icelandic Current Around Iceland. *Journal of Geophysical*
452 *Research: Oceans* 125(9). <https://doi-org.proxy.findit.cvt.dk/10.1029/2020JC016283>
453
- 454 Chafik, L. (2019). *North Atlantic subpolar gyre index. Dataset version 3.0. Bolin Centre*
455 *Database*. <https://doi.org/10.17043/chafik-2019-3>
456
- 457 Chen, W. Y., & van den Dool, H. (2003). Sensitivity of teleconnection patterns to the sign of
458 their primary action center. *Monthly Weather Review*, 131(11), 2885–2899.
459 [https://doi.org/10.1175/1520-0493\(2003\)131<2885:SOTPTT>2.0.CO;2](https://doi.org/10.1175/1520-0493(2003)131<2885:SOTPTT>2.0.CO;2)
460
- 461 Chen, X., & Tung, K. K. (2018). Global surface warming enhanced by weak Atlantic
462 overturning circulation. *Nature*, 559(7714), 387–391. <https://doi.org/10.1038/s41586-018-0320-y>
463
- 464 Daniault, N., Mercier, H., Lherminier, P., Sarafanov, A., Falina, A., Zunino, P., Pérez, F. F.,
465 Ríos, A. F., Ferron, B., Huck, T., Thierry, V., & Gladyshev, S. (2016). The northern North
466 Atlantic Ocean mean circulation in the early 21st century. *Progress in Oceanography*, 146, 142–
467 158. <https://doi.org/10.1016/j.pocean.2016.06.007>
468
- 469 de Jong, M. F., & de Steur, L. (2016). Strong winter cooling over the Irminger Sea in winter
470 2014-2015, exceptional deep convection, and the emergence of anomalously low SST.
471 *Geophysical Research Letters*, 43(13), 7106–7113. <https://doi.org/10.1002/2016GL069596>
472
- 473 Dee, D. P., Balmaseda, M., Balsamo, G., Engelen, R., Simmons, A. J., & Thépaut, J. N. (2014).
474 Toward a consistent reanalysis of the climate system. *Bulletin of the American Meteorological*
475 *Society*, 95(8), 1235–1248. <https://doi.org/10.1175/BAMS-D-13-00043.1>
476

- 477 Desbruyères, D., Chafik, L., & Maze, G. (2021). A shift in the ocean circulation has warmed the
478 subpolar North Atlantic Ocean since 2016. *Communications Earth & Environment* 2021 2:1,
479 2(1), 1–9. <https://doi.org/10.1038/s43247-021-00120-y>
480
- 481 Deser, C., Alexander, M. A., Xie, S.-P., & Phillips, A. S. (2010). Sea Surface Temperature
482 Variability: Patterns and Mechanisms. *Annual Review of Marine Science*, 2(1), 115–143.
483 <https://doi.org/10.1146/annurev-marine-120408-151453>
484
- 485 Dickson, R. R., Osborn, T. J., Hurrell, J. W., Meincke, J., Blindheim, J., Adlandsvik, B., Vinje,
486 T., Alekseev, G., & Maslowski, W. (2000). The Arctic Ocean Response to the North Atlantic
487 Oscillation, *Journal of Climate*, 13(15), 2671-2696. [https://doi.org/10.1175/1520-](https://doi.org/10.1175/1520-0442(2000)013<2671:TAORTT>2.0.CO;2)
488 [0442\(2000\)013<2671:TAORTT>2.0.CO;2](https://doi.org/10.1175/1520-0442(2000)013<2671:TAORTT>2.0.CO;2)
489
- 490 Donlon, C. J., Martin, M., Stark, J., Roberts-Jones, J., Fiedler, E., & Wimmer, W. (2012). The
491 Operational Sea Surface Temperature and Sea Ice Analysis (OSTIA) system. *Remote Sensing of*
492 *Environment*, 116, 140–158. <https://doi.org/10.1016/j.rse.2010.10.017>
493
- 494 Furevik, T. (2000). On Anomalous Sea Surface Temperatures in the Nordic Seas, *Journal of*
495 *Climate*, 13(5), 1044-1053. [https://journals.ametsoc.org/view/journals/clim/13/5/1520-](https://journals.ametsoc.org/view/journals/clim/13/5/1520-0442_2000_013_1044_oassti_2.0.co_2.xml)
496 [0442_2000_013_1044_oassti_2.0.co_2.xml](https://journals.ametsoc.org/view/journals/clim/13/5/1520-0442_2000_013_1044_oassti_2.0.co_2.xml)
497
- 498
- 499 Good, S., Fiedler, E., Mao, C., Martin, M. J., Maycock, A., Reid, R., Roberts-Jones, J., Searle,
500 T., Waters, J., While, J., & Worsfold, M. (2020). The current configuration of the OSTIA system
501 for operational production of foundation sea surface temperature and ice concentration analyses.
502 *Remote Sensing*, 12(4). <https://doi.org/10.3390/RS12040720>
503
- 504 Hansen. B. & Østerhus. (2000). S. North Atlantic-Nordic Seas exchanges. *Progress in*
505 *Oceanography*, 45(2), 109-208. [https://doi.org/10.1016/S0079-6611\(99\)00052-X](https://doi.org/10.1016/S0079-6611(99)00052-X)
506

- 507 Hattermann, T., Isachsen, P. E., von Appen, W.-J., Albretsen, J., and Sundfjord, A. (2016),
508 *Eddy-driven recirculation of Atlantic Water in Fram Strait*, *Geophys. Res. Lett.*, *43*, 3406– 3414,
509 doi:10.1002/2016GL068323.
- 510
- 511 Häkkinen, S., & Rhines, P. B. (2004). Decline of Subpolar North Atlantic Circulation during the
512 1990s. *Science*, *304*(5670), 555–559. <https://doi.org/10.1126/science.1094917>
- 513
- 514 Häkkinen, S., Rhines, P. B., & Worthen, D. L. (2011). Warm and saline events embedded in the
515 meridional circulation of the northern North Atlantic. *Journal of Geophysical Research: Oceans*,
516 *116*(3), 3006. <https://doi.org/10.1029/2010JC006275>
- 517
- 518 Hátún, H., Payne, M. R., Beaugrand, G., Reid, P. C., Sandø, A. B., Drange, H., Hansen, B.,
519 Jacobsen, J. A., & Bloch, D. (2009). Large bio-geographical shifts in the north-eastern Atlantic
520 Ocean: From the subpolar gyre, via plankton, to blue whiting and pilot whales. *Progress in*
521 *Oceanography*, *80*(3–4), 149–162. <https://doi.org/10.1016/j.pocean.2009.03.001>
- 522
- 523 Hátún, H., Sande, A. B., Drange, H., Hansen, B., & Valdimarsson, H. (2005). Ocean science:
524 Influence of the atlantic subpolar gyre on the thermohaline circulation. *Science*, *309*(5742),
525 1841–1844. <https://doi.org/10.1126/science.1114777>
- 526
- 527 Hersbach, H., Bell, B., Berrisford, P., Biavati, G., Horányi, A., Muñoz Sabater, J., Nicolas, J.,
528 Peubey, C., Radu, R., Rozum, I., Schepers, D., Simmons, A., Soci, C., Dee, D., Thépaut, J-N.
529 (2018): ERA5 hourly data on single levels from 1979 to present. Copernicus Climate Change
530 Service (C3S) Climate Data Store (CDS). (Accessed on 14-Jun-2021), 10.24381/cds.adbb2d47
- 531
- 532 Holliday, N. P., Hughes, S. L., Bacon, S., Beszczynska-Möller, A., Hansen, B., Lavín, A.,
533 Loeng, H., Mork, K. A., Østerhus, S., Sherwin, T., & Walczowski, W. (2008). Reversal of the
534 1960s to 1990s freshening trend in the northeast North Atlantic and Nordic Seas. *Geophysical*
535 *Research Letters*, *35*(3). <https://doi.org/10.1029/2007GL032675>

536

- 537 Hurrell, J. W. (1995). Decadal Trends in the North Atlantic Oscillation: Regional Temperatures
538 and Precipitation. *Science*, 269(5224), 676–679. <https://doi.org/10.1126/SCIENCE.269.5224.676>
539
- 540 Jeansson, E., Olsen, A., & Jutterström, S. (2017). Arctic Intermediate Water in the Nordic Seas,
541 1991–2009. *Deep-Sea Research Part I: Oceanographic Research Papers*, 128(March 2016), 82–
542 97. <https://doi.org/10.1016/j.dsr.2017.08.013>
543
- 544 Jónsson, S. & Valdimarsson, H. (2012). Water mass transport variability to the North Icelandic
545 shelf, 1994–2010. *ICES Journal of Marine Science*, 69(5), 809–815.
546 <https://doi.org/10.1093/icesjms/fss024>
547
- 548 Kenigson, J. S., & Timmermans, M. L. (2021). Nordic seas hydrography in the context of arctic
549 and north atlantic ocean dynamics. *Journal of Physical Oceanography*, 51(1), 101–114.
550 <https://doi.org/10.1175/JPO-D-20-0071.1>
551
- 552 Lentz, S. J., & Largier, J. (2006). The influence of wind forcing on the Chesapeake Bay buoyant
553 coastal current. *Journal of Physical Oceanography*, 36(7), 1305–1316.
554 <https://doi.org/10.1175/JPO2909.1>
555
- 556 Lozier, M. S., & Stewart, N. M. (2008). On the temporally varying northward penetration of
557 mediterranean overflow water and eastward penetration of Labrador sea water. *Journal of*
558 *Physical Oceanography*, 38(9), 2097–2103. <https://doi.org/10.1175/2008JPO3908.1>
559
- 560 Masson-Delmotte, V., Zhai, P., Pörtner, H.-O., Roberts, D., Skea, J., Shukla, P. R., Pirani, A.,
561 Moufouma-Okia, W., Péan, C., Pidcock, R., Connors, S., Matthews, J. B. R., Chen, Y., Zhou, X.,
562 Gomis, M. I., Lonnoy, E., Maycock, T., Tignor, M., & Waterfield, T. (2019). Global warming of
563 1.5°C An IPCC Special Report on the impacts of global warming of 1.5°C above pre-industrial
564 levels and related global greenhouse gas emission pathways, in the context of strengthening the
565 global response to the threat of climate change, sustainable development, and efforts to eradicate
566 poverty. Edited by Science Officer Science Assistant Graphics Officer Working Group I
567 Technical Support Unit. In *Nature* (Vol. 291, Issue 5813). <https://doi.org/10.1038/291285a0>

568

569

570

571 Meredith, M. et al. (2019). Polar Regions. In: IPCC Special Report on the Ocean and Cryosphere
572 in a Changing Climate [H.-O. Pörtner, D.C. Roberts, V. Masson-Delmotte, P. Zhai, M. Tignor,
573 E. Poloczanska, K. Mintenbeck, A. Alegría, M. Nicolai, A. Okem, J. Petzold, B. Rama, N.M.
574 Weyer (eds.)]. In press. (Accessed on 07-03-2022 via:

575 <https://www.ipcc.ch/srocc/chapter/chapter-3-2/citation/>)

576 Mikhailova, N. v., Bayankina, T. M., & Sizov, A. A. (2021). Two Modes of Atmosphere–Ocean
577 Interaction in the Atlantic Sector of the Arctic Basin. *Oceanology* 2021 61:4, 61(4), 443–449.

578 <https://doi.org/10.1134/S0001437021030097>

579

580

581

582 Orvik, K. A., & Niiler, P. (2002). Major pathways of Atlantic water in the northern North
583 Atlantic and Nordic Seas toward Arctic. *Geophysical Research Letters*, 29(19).

584 <https://doi.org/10.1029/2002GL015002>

585

586 Raj, R. P., Chatterjee, S., Bertino, L., Turiel, A., & Portabella, M. (2019). The Arctic Front and
587 its variability in the Norwegian Sea. *Ocean Science*, 15(6), 1729–1744.

588 <https://doi.org/10.5194/OS-15-1729-2019>

589

590

591

592 Sandø, A. B., Nilsen, J. E. Ø. and Bentsen, M. (2012). Mechanisms for variable North Atlantic-
593 Nordic seas exchanges. *Journal of Geophysical Research: Oceans*, 117(12). <https://doi->

594 [org.proxy.findit.cvt.dk/10.1029/2012JC008177](https://doi.org.proxy.findit.cvt.dk/10.1029/2012JC008177)

595

596 Serreze, M. C., Barrett, A. P., Slater, A. G., Steele, M., Zhang, J., & Trenberth, K. E. (2007). The
597 large-scale energy budget of the Arctic. *Journal of Geophysical Research Atmospheres*, 112(11).

598 <https://doi.org/10.1029/2006JD008230>

599

600 Smedsrud, L. H., Muilwijk, M., Brakstad, A., Madonna, E., Lauvset, S. K., Spensberger, C.,
601 Born, A., Eldevik, T., Drange, H., Jeansson, E., Li, C., Olsen, A., Skagseth, Ø., Slater, D. A.,
602 Straneo, F., Våge, K., & Årthun, M. (2022). Nordic Seas Heat Loss, Atlantic Inflow, and Arctic
603 Sea Ice Cover Over the Last Century. *Reviews of Geophysics*, *60*(1), e2020RG000725.
604 <https://doi.org/10.1029/2020RG000725>

605

606 Somavilla, R., González-Pola, C., & Fernández-Díaz, J. (2017). The warmer the ocean surface,
607 the shallower the mixed layer. How much of this is true? *Journal of Geophysical Research:*
608 *Oceans*, *122*(9), 7698–7716. <https://doi.org/10.1002/2017JC013125>

609

610

611

612 Stark, J. D., Donlon, C. J., Martin, M. J., & McCulloch, M. E. (2007). OSTIA: An operational,
613 high resolution, real time, global sea surface temperature analysis system. *OCEANS 2007 -*
614 *Europe*. <https://doi.org/10.1109/OCEANSE.2007.4302251>

615

616 Sutherland, D. A., & Pickart, R. S. (2008). The East Greenland Coastal Current: Structure,
617 variability, and forcing. *Progress in Oceanography*, *78*(1), 58–77.
618 <https://doi.org/10.1016/j.pocean.2007.09.006>

619 Sarafanov, A. (2009). On the effect of the north Atlantic oscillation on temperature and salinity
620 of the subpolar north Atlantic intermediate and deep waters. *ICES Journal of Marine Science*,
621 *66*(7), 1448–1454. <https://doi.org/10.1093/ICESJMS/FSP094>

622

623 Tsubouchi, T., Våge, K., Hansen, B., Larsen, K. M. H., Østerhus, S., Johnson, C., Jónsson, S., &
624 Valdimarsson, H. (2021). Increased ocean heat transport into the Nordic Seas and Arctic Ocean
625 over the period 1993–2016. *Nature Climate Change*, *11*(1), 21–26.
626 <https://doi.org/10.1038/s41558-020-00941-3>

627

628 van den Dool, H. M., Saha, S., & Johansson, Å. (2000). Empirical orthogonal teleconnections.
629 *Journal of Climate*, 13(8), 1421–1435. <https://doi.org/10.1175/1520->

630 0442(2000)013<1421:EOT>2.0.CO;2

631 Visbeck, M., Chassignet, E. P., Curry, R. G., Delworth, T. L., Dickson, R. R., & Krahnemann, G.
632 (2003). The Ocean's Response to North Atlantic Oscillation Variability. *Geophysical*

633 *Monograph Series*, 134, 113–145. <https://doi.org/10.1029/134GM06>

634

635 Zhao, J., Yang, S. & Semper, S. A. (2018). Numerical Study of Interannual Variability in the

636 North Iceland Irminger Current. *Journal of Geophysical Research: Oceans*, 123(12), 8994-9009.

637 <https://doi-org.proxy.findit.cvt.dk/10.1029/2018JC013800>

638

639 Østerhus, S., Woodgate, R., Valdimarsson, H., Turrell, B., de Steur, L., Quadfasel, D., Olsen, S.

640 M., Moritz, M., Lee, C. M., Larsen, K. M. H., Jónsson, S., Johnson, C., Jochumsen, K., Hansen,

641 B., Curry, B., Cunningham, S., & Berx, B. (2019). Arctic Mediterranean exchanges: A consistent

642 volume budget and trends in transports from two decades of observations. *Ocean Science*, 15(2),

643 379–399. <https://doi.org/10.5194/OS-15-379-2019>

644

645

646 **Table 1.** SST datasets and their key characteristics used in this study.

Dataset type	Parameter	Coverage	Temporal resolution	Timespan in study	Spatial resolution
OSTIA near-real time	Foundation SST	Global	Daily	2007-2020	0.05°
	Sea-ice fraction	Gloabl	Daily	2007-2020	0.05°
	Analysis error	Global	Daily	2007-2020	0.05°
ERA5 Reanalysis	Foundation SST	Global	Hourly	1979-2020	0.25°
	Sea-ice fraction	Global	Hourly	1979-2020	0.25°

647

648

649 **Figure Legends**

650 **Figure 1.** Average Sea Surface Temperature calculated from 2007-2020 daily values derived
651 from “Operational Sea Surface Temperature and Sea Ice Analysis (OSTIA)”, developed by the
652 Met Office (Table 1). Yellow contours indicate the 500 m isobath and red and grey arrows
653 indicate major warm and cold surface circulation features in the region, respectively. The
654 position of the Siglunes transect is denoted by the triangle on the north Iceland shelf.

655 **Figure 2.** Results of a linear regression across the OSTIA dataset from 2007-2020 segregated by
656 season: Winter (December to February); spring (March to May); summer (June to August) and
657 autumn (September to November). Top row shows the slope of the regression. Isolines indicate

658 the division between significant ($p < 0.05$) and non-significant regression slopes. The bottom row
659 presents maps of the p-value for the regressions.

660 **Figure 3.** First four Empirical Orthogonal Functions derived from the analysis of the ERA5 SST
661 dataset. The maps to the left indicate the geographical loadings and the plots on the right
662 represent the contribution of each component to the SST anomaly for selected locations (red and
663 black). The locations for the plotted SST anomalies are shown on each of the maps (red and
664 black dot).

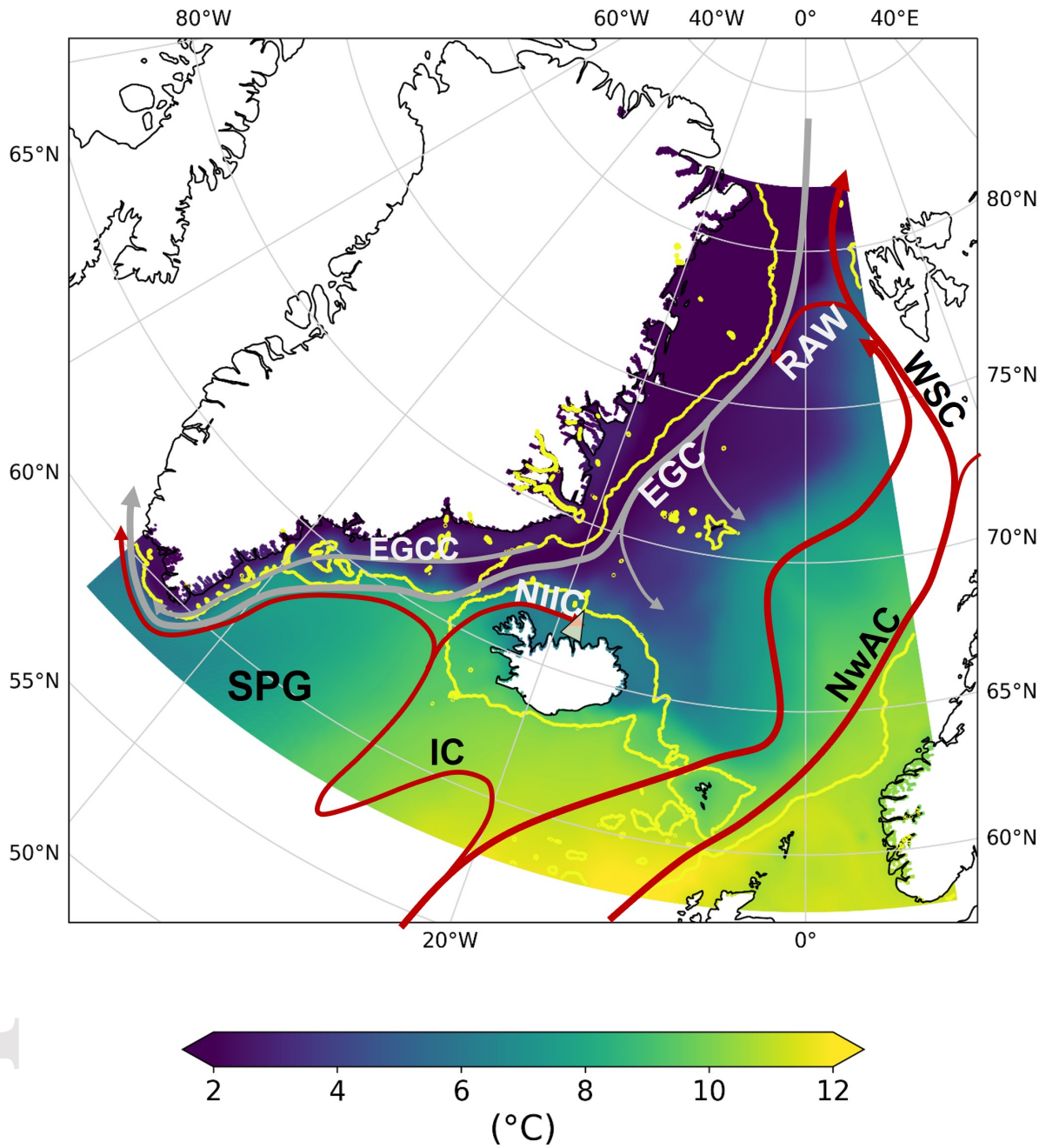
665 **Figure 4.** Analysis of temporal developments in the seasonality represented by EOF1. A)
666 Hovmöller plot of the development of temperature anomaly assigned to EOF1 across the year
667 and over the time series. Grey and yellow lines represent the timing of the summer maximum
668 and winter minimum, respectively. B) Development of the annual summer maxima and winter
669 minima across the time series. C) Analysis of de-seasoned scores revealing two distinct periods.
670 Linear regression lines are presented for the period 1979-2000 (orange line) and the period 2000-
671 2020 (green line).

672 **Figure 5.** Comparison of the time series of EOF2 with NAO and SPG. Cross-correlation analysis
673 of EOF2 with NAO (A) and SPG (C) revealed a 4 and 5-week lag, respectively. Panels B and D
674 compare EOF2 and the two indices. A 12 week rolling average with a cosine window is applied
675 on both the EOF2 and the NAO and SPG time series. Both NAO and SPG were recalculated
676 from monthly to weekly time series. The vertical lines in panels B and D (1995 and 2014) mark
677 transition in the NAO and SPG indices.

678 **Figure 6.** Weekly mean seasonal SST anomalies explained by EOF3 in the Irminger Sea [31°W ,
679 65°N , Fig. 3e red dot] averaged over 5 year intervals.

680 **Figure 7.** Normalized mean August temperature at the Siglunes transect (blue) and SST
681 anomalies induced by EOF4 at the same location (red). Data from the Siglunes transect at
682 approx. 67.75°N , 18.83°W (triangle on Fig. 1) collected by the Marine and Freshwater
683 Research Institute were downloaded from SeaDataNet (<https://cdi.seadatanet.org/search>).

684



This article has been accepted for publication and undergone full peer review but has not been through the copyediting, typesetting, pagination and proofreading process, which may lead to differences between this version and the [Version of Record](https://doi.org/10.1029/2022JC018630). Please cite this article as [doi: 10.1029/2022JC018630](https://doi.org/10.1029/2022JC018630).

This article is protected by copyright. All rights reserved.

